Contents lists available at ScienceDirect

Biomedicine & Pharmacotherapy

journal homepage: www.elsevier.com/locate/biopha

Preclinical validation of a new hybrid molecule loaded in liposomes for melanoma management

Jacinta O. Pinho [a], Mariana Matias [a], Vanda Marques [a], Carla Eleutério [a], Célia Fernandes [b], Lurdes Gano [b], Joana D. Amaral [a], Eduarda Mendes [a], Maria Jesus Perry [a], João Nuno Moreira [c,d], Gert Storm [e,f,g], Ana Paula Francisco [a], Cecília M.P. Rodrigues [a], M. Manuela Gaspar [a,*]

[a] Research Institute for Medicines, iMed.ULisboa, Faculty of Pharmacy, Universidade de Lisboa, Av. Prof. Gama Pinto, 1649-003 Lisboa, Portugal
[b] Centro de Ciências e Tecnologias Nucleares e Departamento de Engenharia e Ciências Nucleares, Instituto Superior Técnico, Universidade de Lisboa, Bobadela LRS, Portugal
[c] Center for Neurosciences and Cell Biology (CNC), Center for Innovative Biomedicine and Biotechnology (CIBB), University of Coimbra, Faculty of Medicine (Polo 1), Rua Larga, 3004-504 Coimbra, Portugal
[d] University of Coimbra (Univ Coimbra), CIBB, Faculty of Pharmacy, Pólo das Ciências da Saúde, Azinhaga de Santa Comba, 3000-548 Coimbra, Portugal
[e] Department of Pharmaceutics, Utrecht Institute for Pharmaceutical Sciences, Utrecht University, Utrecht, the Netherlands
[f] Department of Biomaterial Science and Technology, University of Twente, Enschede, the Netherlands
[g] Department of Surgery, Yong Loo Lin School of Medicine, National University of Singapore, Singapore 119228, Singapore

ARTICLE INFO

ABSTRACT

The aggressiveness of melanoma and lack of effective therapies incite the discovery of novel strategies. Recently, a new dual acting hybrid molecule (HM), combining a triazene and a L-tyrosine analogue, was synthesized. HM was designed to specifically be activated by tyrosinase, the enzyme involved in melanin biosynthesis and overexpressed in melanoma. HM displayed remarkable superior antiproliferative activity towards various cancer cell lines compared with temozolomide (TMZ), a triazene drug in clinical use, that acts through DNA alkylation. In B16-F10 cells, HM induced a cell cycle arrest at phase G0/G1 with a 2.8-fold decrease in cell proliferation index. Also, compared to control cells, HM led to a concentration-dependent reduction in tyrosinase activity and increase in caspase 3/7 activity. To maximize the therapeutic performance of HM *in vivo*, its incorporation in long blood circulating liposomes, containing poly(ethylene glycol) (PEG) at their surface, was performed for passively targeting tumour sites. HM liposomes (LIP HM) exhibited high stability in biological fluids. Preclinical studies demonstrated its safety for systemic administration and in a subcutaneous murine melanoma model, significantly reduced tumour progression. In a metastatic murine melanoma model, a superior antitumour effect was also observed for mice receiving LIP HM, with markedly reduction of lung metastases compared to positive control group (TMZ). Biodistribution studies using ^{111}In-labelled LIP HM demonstrated its ability for passively targeting tumour sites, thus correlating with the high therapeutic effect observed in the two experimental murine melanoma models. Overall, our proposed nanotherapeutic strategy was validated as an effective and safe alternative against melanoma.

1. Introduction

Melanoma is an aggressive skin malignancy, with rising incidence and mortality worldwide [1]. The current limitations of available therapeutic options are very concerning and encourage the search for new and more effective therapies [2]. In this context, molecular hybridization is a synthetic approach in medicinal chemistry and represents a promising research strategy to develop novel drug candidates [3–5]. Hybrid molecules result from covalent fusion of two or more distinct pharmacophores to produce a single compound. They act simultaneously on different pharmacological targets, aiming to potentiate therapeutic effects and to reduce drug resistance [4,5]. The therapeutic potential of this strategy is demonstrated by examples of hybrid molecules with anticancer properties currently used in clinical practice [6]. This is the case of estramustine, approved for the palliative care of patients with metastatic and/or progressive prostate carcinoma, or midostaurin, indicated for FMS-like tyrosine kinase 3 (FLT3)-mutated acute myeloid leukaemia and aggressive systemic mastocytosis [6–8].

Regarding melanoma, triazenes constitute an important class of molecules with well documented anticancer properties [5,9,10]. The most clinically relevant triazene drugs are dacarbazine and its oral derivative, temozolomide (TMZ), used to treat advanced melanoma *via* DNA alkylation [5,11,12]. Recently, hybrid molecules composed of two pharmacophores, a triazene with DNA alkylating properties and the L-tyrosine analogue, 4-*S*-cysteaminylphenol (4-*S*-CAP) acting as a tyrosinase substrate, were designed [13]. The rational for the design of these hybrid molecules is to specifically reach melanoma sites, promoting their *in situ* activation by overexpressed tyrosinase and release of cytotoxic compounds [14,15]. Series of these hybrid molecules demonstrated promising *in vitro* antimelanoma activity, reinforcing the importance of the dual mechanism of action [13].

When considering the *in vivo* applications of potential antimelanoma hybrid molecules, the enhancement of their pharmacological properties is of utmost importance. For this purpose, resorting to nanotechnological tools for the delivery of therapeutic agents is a frequently employed strategy [16–19]. Liposomes, in particular, are an attractive, versatile and clinically well-known lipid-based nanosystem suitable for loading both hydrophobic and hydrophilic molecules [20]. Moreover, liposomes can be coated with poly(ethylene glycol) (PEG), a widely described approach able to increase stability and prolong blood circulating times as a result of reduced adsorption of plasmatic proteins at their surface, thus enabling their passive extravasation to tumour sites [21–24]. On the other hand, the presence of a high variety of ligands onto liposome surface enables the active targeting of tumours through the specific recognition of overexpressed receptors at these sites [20]. The clinical success of this lipid-based system is evidenced by several approved liposomal formulations [2,25,26]. Liposomes have been shown to be able to solubilize poorly water soluble compounds, to prevent premature degradation of loaded molecules, and to accumulate preferentially at diseased sites leading to enhanced therapeutic efficacy [2,20,26–28]. Liposomal formulations have advantages over many other nanoparticulate systems as they are mainly composed of natural lipids that are biocompatible, biodegradable, non-immunogenic, and therefore preferred from a toxicological point of view. Also, they are familiar to the scientific community, Food and Drug Administration (FDA) and European Medicines Agency (EMA).

Inspired by the encouraging anticancer properties of a newly synthesized set of hybrid molecules [13], the most promising one, hereafter referred to as HM, was selected for further evaluation. Using melanoma cell lines, we investigated the antiproliferative properties of HM, its effect on cell cycle distribution, caspase 3/7 and tyrosinase activity. Aiming to maximize its passive accumulation at tumour sites, HM was incorporated in long blood circulating liposomes. HM liposomes proved to be stable in the bloodstream, without induction of haemolysis. The therapeutic effect of nanoformulated HM was validated in both syngeneic subcutaneous and metastatic melanoma murine models. Moreover, the biodistribution of HM liposomes was assessed in both murine melanoma models.

2. Material and methods

2.1. Materials

The reagents dimethyl sulfoxide (DMSO), 3-(4,5-dimethylthiazol-2-yl)− 2,5-diphenyltetrazolium bromide (MTT) and mushroom tyrosinase were purchased from Sigma-Aldrich (St Louis, MO, USA); temozolomide (TMZ) was acquired from TCI (Nihonbashi-honchou, Tokyo), and L-DOPA was purchased from Alfa Aesar (Kandel, Germany). Culture media and antibiotics were obtained from Invitrogen (Life Technologies Corporation, NY, USA). Reagents for cell proliferation assays were purchased from Promega (WI, USA). The pure phospholipids egg phosphatidyl choline (EPC), distearoyl phosphatidyl ethanolamine covalently linked to polyethylene glycol 2000 (DSPE-PEG), DSPE-PEG covalently linked to folic acid (DSPE-PEG-FA) and dioleoyl phosphatidyl ethanolamine (DOPE), used for the preparation of liposomal nanoformulations, were purchased from Avanti Polar Lipids (AL, USA). All the remaining chemicals used were of analytical grade. Deionized water (Milli-Q system; Millipore, Tokyo) was used in all experiments.

2.2. Cell culture

Supplementary Information.

2.3. MTT assay

Cell viability was evaluated in the absence (control) or presence of increasing concentrations of HM and TMZ by the MTT assay. After reaching around 80% confluence, B16-F10, A375, MNT-1 and HaCaT cells were gently detached and counted using the trypan blue dye exclusion method. Then, 5×10^4 cells were seeded in 96-well culture plates and allowed to attach for 24 h. After that, the culture medium was replaced by fresh medium containing HM or TMZ (positive control) at concentrations ranging from 10 to 75 μM, for 24, 48 and 72 h, or complete medium (negative control). After the respective incubation period, the medium was removed, and cells were washed twice (200 μL/well) with phosphate buffered saline (PBS). Subsequently, 50 μL of the MTT solution (0.5 mg/mL), prepared in the appropriate serum-free medium, was added to each well, followed by a 3 h incubation at + 37 °C. The resulting formazan crystals were dissolved in DMSO and the absorbance was measured at 570 nm using a microplate reader Model 680 (Bio-Rad, CA, USA). Cell proliferation analysis was carried out in GraphPad Prism®5 (GraphPad Software, CA, USA). Values were plotted and fit to a standard inhibition log concentration-response curve to generate the IC_{50} values.

2.4. Guava ViaCount assay

Supplementary Information.

2.5. Cell cycle distribution

Supplementary Information.

2.6. Caspase 3/7 activity

Supplementary Information.

2.7. Tyrosinase activity

Supplementary Information.

2.8. Liposomes preparation

Liposomes were prepared by the dehydration–rehydration method [29]. An initial lipid concentration of 30 μmol/mL was used. Briefly, the selected phospholipids and HM at a concentration of 1 μmol/mL were dissolved in chloroform, which was further evaporated (Buchi R-200 rotary evaporator, Switzerland) to obtain a thin lipid film in a round-bottomed flask. For fluorescently labelled liposomes, rhodamine covalently linked to phosphatidyl ethanolamine was included in the lipid mixture at 0.1 mol% related to total lipid. The obtained lipid film was dispersed with deionized water and the so-formed suspension was frozen (−70 °C) and lyophilized (freeze–dryer, CO, USA) overnight. The rehydration of the lyophilized powder was performed in HEPES buffer pH 7.4 (10 mM HEPES, 140 mM NaCl) in two steps, to maximize HM incorporation. The so-formed liposomal suspension was then filtered, under nitrogen pressure (10–500 lb/in^2), through polycarbonate membranes of appropriate pore size until an average vesicle size of 100 nm was obtained, using an extruder device (Lipex: Biomembranes Inc., Vancouver, Canada). The separation of non-incorporated HM was performed by gel filtration (Econo-Pac® 10DG; Bio-Rad Laboratories, Hercules, CA), followed by ultracentrifugation at 250,000 *g*, for 120 min, at + 15 °C in a Beckman LM-80 ultracentrifuge (Beckman Instruments, Inc, CA, USA). Finally, the pellet was suspended in HEPES buffer pH 7.4.

2.9. Liposomes characterization

Liposomes were characterized in terms of incorporation parameters, mean size and surface charge. Loading capacity was defined as the final HM to lipid ratio (HM/Lip)f and the incorporation efficiency (I.E.), in percentage, was determined using the Eq. (1):

$$\text{I.E. } (\%) = \frac{\left(\frac{\text{HM}}{\text{Lip}}\right)\text{f}}{\left(\frac{\text{HM}}{\text{Lip}}\right)\text{i}} \times 100 \tag{1}$$

Phosphate content was measured using a colorimetric technique described by Rouser [30]. Liposomes mean size and polydispersity index (PdI) were determined by dynamic light scattering (Zetasizer Nano Series, Nano-S Malvern Instruments, Malvern, UK) at a standard laser wavelength of 663 nm. Zeta potential of liposomal formulations was measured in a hydrodynamic sizing system (Zetasizer nano Series Nano-Z Malvern Instruments, Malvern, UK).

2.10. HM quantification

The quantification of HM was performed by high performance liquid chromatography (HPLC). The HPLC system was an ELITE LaChrom Hitachi (Japan), comprising a L-2130 pump module, a Diode-Array L-2455 detector and an autosampler L-2200 with a loop of 20 μL. The wavelength of the detector was set at 300 nm. The system was connected to a computer with specific software, Ez Chrom Elite, for integration and treatment of chromatograms. The analytical column was a LiChroCART® (150−4,6) Purospher® Star RP-18 (5 μm) (Merck) equipped with the respective guard-column. The mobile phase, in an isocratic solvent system, consisted of acetonitrile (ACN)/water (H$_2$O) [50:50 (*v/v*)], with a flow rate of 1 mL/min at + 25 °C. Linearity of calibration curves was ensured from 1.25 to 20 μM (R^2 = 0.9998). Samples were appropriately diluted in ACN in the range of the respective calibration curve.

2.11. Internalization of HM liposomes

Supplementary Information.

2.12. Stability of liposomal HM

The stability of HM liposomes in suspension was assessed by quantifying HM and lipid contents after storage at + 4 °C, for 1 week (day 7). Following this period, samples were submitted to gel filtration and ultracentrifuged at 250,000 *g*, for 120 min, at + 15 °C. Liposomes were suspended in HEPES buffer pH 7.4, and HM and phospholipid contents were quantified. The stability was defined as the ratio, in percentage, between HM to lipid ratio after 1 week of storage (day 7) and the initial HM to lipid ratio (day 0), according to the Eq. (2). Mean size, PdI and zeta potential were also determined for all samples.

$$\text{HM associated to liposomes } (\%) = \frac{\left(\frac{\text{HM}}{\text{Lip}}\right)day7}{\left(\frac{\text{HM}}{\text{Lip}}\right)day0} \times 100 \tag{2}$$

The stability of HM liposomes in the lyophilized form was assessed in the absence and presence of the cryoprotectant trehalose [29]. Briefly, HM liposomes were prepared using the same method described above, using HEPES buffer pH 7.4 or 10 mM HEPES, 280 mM trehalose, pH 7.4 in rehydration steps, respectively. The two different buffers were used for suspending the respective liposomes after the ultracentrifugation step (preceded by extrusion and gel filtration). Then, liposomes were lyophilized and stored at + 4 °C. After 1 month, liposomes were rehydrated with water (same volume as the one previously lyophilized) and the percentage of HM still associated to liposomes was quantified. For that, HM liposomes were diluted in HEPES buffer pH 7.4 and submitted to gel filtration, followed by ultracentrifugation at 250,000 *g*, for 120 min, at + 15 °C. The obtained pellets were suspended in HEPES buffer pH 7.4, and HM and phospholipid contents were determined. Stability was defined as the ratio, in percentage, between HM to lipid ratio after 1 month of storage (day 30) and the initial HM to lipid ratio (day 0), according to the Eq. (3). Mean size, PdI and zeta potential of samples were also determined.

$$\text{HM associated to liposomes } (\%) = \frac{\left(\frac{\text{HM}}{\text{Lip}}\right)day30}{\left(\frac{\text{HM}}{\text{Lip}}\right)day0} \times 100 \tag{3}$$

2.13. Stability of LIP HM in human plasma

Supplementary Information.

2.14. Human plasma stability

The hydrolysis rate of HM incorporated in liposomes and the appearance of the sub-products was performed following incubation in human plasma [80% (*v/v*) diluted in HEPES buffer pH 7.4 and incubated at + 37 °C], obtained from different healthy individuals and pooled [9]. The reactions were monitored by HPLC technique, which revealed the reduction of the HM and the appearance of hydrolysis sub-products. The HM hydrolysis reaction was monitored until achieving at least three half-lives of the compound. Briefly, the mixture containing human plasma and HM in free and liposomal forms was incubated at + 37 °C and, at pre-selected times, aliquots of 100 μL were removed from the plasma medium, diluted with 900 μL of ACN, centrifuged and the supernatant injected into HPLC column for quantification.

2.15. Haemolysis assay

The haemolytic activity of HM in free and liposomal forms, as well as unloaded liposomes, was determined using EDTA-preserved peripheral human blood, obtained from voluntary donors and used in the same day of experiments [31]. Plasma was firstly removed by centrifugation at 1000 *g*, for 10 min and, after, erythrocyte suspension was washed three times in PBS, at 1000 *g*, for 10 min. HM concentrations ranging from 0.2 to 400 μM were distributed in 96-well plates (100 μL/well). Then,

100 µL of erythrocyte suspension was added to all wells, incubated at + 37 °C for 1 h, and centrifuged at 800 g for 10 min. Absorbance of supernatants was measured at 550 nm with a reference filter at 620 nm. The percentage of the haemolytic activity for each sample was calculated comparing each individual determination to a positive control, corresponding to 100% haemolysis (erythrocytes incubated with distilled water) and negative control (erythrocytes incubated with PBS) according to the Eq. (4), where AbsS is the average absorbance of the sample, AbsN is the average absorbance of the negative control and AbsP is the average absorbance of the positive control.

$$\text{Haemolysis } (\%) \ = \ \frac{(\text{AbsS-AbsN})}{(\text{AbsP-AbsN})} \ \times 100 \quad (4)$$

2.16. Proton nuclear magnetic resonance

Deuterated chloroform ($CDCl_3$) solutions of HM in the free form, unloaded liposomes and HM incorporated in liposomes, were prepared for ^1H NMR experiments recorded at + 20 °C in a Bruker Ultra-Shield 300 MHz spectrometer. HM concentration was the same in both free and liposomal forms and lipid concentration was the same for unloaded and loaded liposomes. Chemical shifts (δ) were reported in parts *per* million (ppm) relative to the residual solvent peak, and the observed changes after formulation of HM in liposomes recorded and analysed.

2.17. Animal studies

Male BALB/c mice 8–10 weeks old were obtained from Gulbenkian Institute of Science (Lisbon, Portugal) and male C57BL/6 mice 8–10 weeks old were purchased from Charles River (Barcelona, Spain). Animals were kept under standard hygiene conditions, fed commercial chow and given acidified drinking water *ad libitum*. All animal experiments were conducted according to the animal welfare organ of the Faculty of Pharmacy, University of Lisbon, approved by the competent national authority *Direção-Geral de Alimentação e Veterinária* (DGAV) and in accordance with the EU Directive (2010/63/UE) and Portuguese laws (DR 113/2013, 2880/2015, 260/2016 and 1/2019) for the use and care of animals in research.

2.18. In vivo toxicity profile in BALB/c mice

Supplementary Information.

2.19. Syngeneic subcutaneous melanoma murine model

For syngeneic tumour induction, a total of 1×10^5 B16-F10 murine melanoma cells were suspended in PBS and injected subcutaneously in the right flank of C57BL/6 male mice. Tumours became palpable around 10–12 days after subcutaneous injection of B16-F10 cells and treatment schedule was initiated. Mice were randomly divided in groups of 8–11 and received the formulations under study by intravenous (i.v.) route, in a total of six administrations every other day. Negative control group received PBS (Control) and the treated groups received HM in the free form (Free HM) or incorporated in long circulating liposomes (LIP HM) at 12 mg of HM/kg of body weight/administration. Mice were monitored every day for pain or distress and body weight was registered. Tumour size was regularly measured using a digital calliper and respective volumes were calculated according to the formula: V (mm^3) = (L×W^2)/2, where L and W represent the longest and shortest axis of the tumour, respectively. Relative tumour volumes (RTVs) were determined for each animal, as the ratio between volumes at the indicated day and volumes at the beginning of the treatment. Three days after the final treatment, mice were sacrificed, blood was collected and primary tumours were excised, weighed and a portion was stored at − 80 °C for further analysis. Spleen, liver, kidneys, and lungs were excised and weighed. Tissue index was calculated according to the Eq. (5):

$$\text{Tissue index } = \ \sqrt{\frac{\text{organ weight}}{\text{animal weight}}} \times 100 \quad (5)$$

Mice were euthanized when they met the ethical euthanasia criteria for tumour size and overall health condition.

2.20. Protocol optimization for syngeneic metastatic melanoma mouse model

Supplementary Information.

2.21. Syngeneic metastatic melanoma murine model

For metastatic tumour induction, a total of 5×10^5 B16-F10 murine melanoma cells were suspended in PBS and injected intravenously in C57BL/6 male mice. Seven days after, mice were randomly divided in groups of 4–6 and received the formulations under study by i.v. route, for five consecutive days. Negative control group received PBS (Control); positive control group received TMZ at 25 mg/kg of body weight/ administration; and HM in the free form (Free HM) or incorporated in long circulating liposomes (LIP HM) was administered at 12 mg/kg body weight/administration. Mice were monitored for pain or distress and weighed. Animals were euthanized when they met the ethical euthanasia criteria for overall health condition (loss of weight > to 20% or demonstrating a morbidity status). Three days after the last administration, mice were sacrificed and blood, lungs and brains were collected for further analysis. Tissue indexes were determined according to the Eq. (5). Lungs were macroscopically analysed, and a score based on the number of metastases was established, where: no metastases = 0; 1–10 = 1; 11–100 = 2; 101–200 = 3; and > 200 = 4.

2.22. Histological analysis

Representative portions of lung and brain tissues were harvested, fixed in 10% buffered formalin, and processed for standard histological analysis. Sections were stained with haematoxylin and eosin and Fontana-Masson (for melanic pigment) for evaluation of pathological changes.

2.23. Ex vivo hepatic biochemical parameters determination

Serum was isolated from the blood and three hepatic enzymes, serum aspartate transaminase (AST), serum alanine transaminase (ALT) and serum γ-glutamyl transferase (γ-GT), were determined using commercially available Kits (Spinreact, Spain), following the manufacturer's instructions.

2.24. Ex vivo caspase 3/7 and tyrosinase activity assays

The enzymatic activity of caspase 3/7 and tyrosinase in protein extracts from mass tumours or lungs from syngeneic subcutaneous and metastatic melanoma models were respectively determined using the same procedure described for cell lines in Supplementary Information.

2.25. Biodistribution studies

The *in vivo* fate of HM liposomes was assessed by labelling liposomes co-incorporating HM and the chelating agent diethylenetriamine pentaacetic acid (DTPA) with a gamma emitting radionuclide, ^{111}In [32]. Radiolabelling and subsequent biodistribution studies were performed at *Campus Tecnológico Nuclear* (CTN) facilities, a Portuguese Institution certified for working with radioactive materials.

DTPA incorporation and Radiolabelling: DTPA at a concentration of 6 µM was incorporated during HM liposomes preparation, after achievement of the lipidic film and before lyophilization. Then, HM

liposomes co-loaded with DTPA were labelled with ^{111}In, using the lipophilic complex ^{111}In-oxine as precursor. The ^{111}In-oxine complex passively crossed the lipid membrane and in the internal aqueous compartment of liposomes transferred the metal ion to DTPA where the hydrophilic complex ^{111}In-DTPA remained trapped.

Biodistribution experiments were performed in 3 different groups of C57BL/6 mice, the subcutaneous and metastatic melanoma models (established as described above) and in healthy mice. Animals were intravenously injected in the tail vein with 100 μL of ^{111}In-labelled HM liposomes and were sacrificed by cervical dislocation at 1, 4, 24 and 48 h post-injection. The administered dose was measured using a dose calibrator (Carpintec CRC-15 W). For each selected time point, 3 mice were sacrificed, blood was collected by cardiac puncture and organs were dissected, rinsed to remove blood excess, weighed, and their radioactivity measured using a γ-counter (Berthold). The results were expressed as the percentage of the injected dose *per* gram of organ, % I.D./g organ, % I.D./total organ or total blood.

2.26. Statistical methods

Data are expressed as mean ± standard deviation (s.d.) for *in vitro* assays and as mean ± standard error mean (s.e.m.) for *ex vivo* and *in vivo* assays. Comparison among groups of one factor was analysed by using Student's *t*-test (two groups) and by one-way or two-way analysis of variance (ANOVA; three or more groups), followed by Dunnett's or Tukey's test. Differences between groups were considered statistically significant when $P < 0.05$. The determination for the IC$_{50}$ was done by sigmoidal fitting analysis considering a confidence level of 95%.

3. Results

3.1. In vitro studies – evaluation of HM mechanisms of action

The present work aims to evaluate the activity of the newly synthesized compound HM, composed of one moiety presenting DNA alkylating properties and another one with tyrosinase specificity, both *in vitro* and *in vivo* [13]. Based on the dual mechanisms of action, it is expected a potentiation of HM anticancer effects compared to the positive control, TMZ, a triazene derivative that acts only through alkylation of DNA bases [5,33].

In vitro studies were conducted using three melanoma cell lines (the murine B16-F10 and human A375 and MNT-1 cell lines) and normal human keratinocytes (HaCaT). Notably, exposure of cells to HM resulted in a concentration- and time-dependent antiproliferative activity superior to that of TMZ, according to the MTT results (Fig. 1a and Supplementary Table S1). The lower IC$_{50}$ values for HM were obtained in A375 cells (40–60 μM), while in B16-F10 and MNT-1 cells, the IC$_{50}$ ranged from 46 to 65 μM and 62 to > 75 μM, respectively (Fig. 1a and Supplementary Table S1). In turn, TMZ displayed marginal cytotoxic properties, as for the maximum concentration tested (75 μM), cell viability was superior to 80% for all timepoints. Finally, in HaCaT cells, HM and TMZ exhibited IC$_{50}$ values between 44 and 60 μM and > 75 μM, respectively (Fig. 1a and Supplementary Table S1). Furthermore, the *in vitro* screening of HM and TMZ in other murine and human cancer cell lines also revealed the superior antiproliferative properties of HM compared to TMZ in all tested conditions (Supplementary Fig. S1).

To further dissect HM mechanisms of action we used the murine B16-F10 melanoma cell line. First, we analysed cell death and viability by flow cytometry, using the Guava ViaCount assay that allows to distinguish between apoptotic and necrotic-like cell death. As depicted in Fig. 1c, approximately 90% of the cells incubated with HM at 50 μM for 24 h were viable, with the remaining cells distributed in 3% apoptotic and 7% necrotic-like. Similar results were obtained for cells treated with 70 μM TMZ after the same period of time (Fig. 1c). Despite the tested concentrations were below the IC$_{50}$ values obtained for those experimental conditions, it was expected to observe higher levels of cell death.

Nevertheless, HM exposure resulted in a strike decrease of cell concentration, corresponding to a reduction of almost 4-fold in the number of cells/μL, compared to control, and around 2-fold relative to TMZ, suggesting a relevant effect of HM in cell proliferation (Fig. 1c). Taking this into account, we next decided to evaluate the cell cycle phase distribution by flow cytometry, using cells stained with PI. Importantly, cell cycle analysis was in agreement with the antiproliferative effect of HM demonstrated by the arrest of cells in the G0/G1 phase (Fig. 1d, e). A 2.3-fold increase in the percentage of cells in G0/G1 phase was achieved following incubation with HM (76%), compared to control (33%) and TMZ (41%). This was accompanied by a concomitant decrease of 3-fold in the percentage of cells in S phase (Fig. 1d, e). These results are clearly reflected by the significant reduction of HM proliferation index compared to control ($p < 0.0001$), while for TMZ such effect was not observed (Fig. 1f).

Finally, we analysed the enzymatic activity of caspase 3/7 and tyrosinase. The first one is responsible for dismantling the dying cell, and the latter is overexpressed in malignant melanoma. These determinations were assessed in whole-cell lysates from B16-F10 cells incubated with HM or TMZ. As observed in Fig. 1g, caspase activity was significantly increased in cells exposed to HM at 50 μM ($p < 0.011$) and TMZ at 70 μM ($p < 0.006$) for 4 h. In addition, our results confirmed that this cell line expresses considerably higher levels of tyrosinase than other melanoma cells, namely MNT-1 and A375 (Supplementary Fig. S2). Importantly, after incubation with HM, a concentration-dependent reduction of tyrosinase activity was observed (Fig. 1h).

3.2. HM liposomes – physicochemical characterization and stability

Liposomes, one of the most successful and safe lipid-based systems, were selected in the present work aiming to improve the stability of loaded HM in bloodstream, promoting a preferential targeting to tumour sites and, consequently, enhance the therapeutic effect. Using the dehydration-rehydration method [29] (Fig. 2a), the hydrophobic compound HM was efficiently incorporated into EPC-based liposomes (Fig. 2b). EPC bilayers are fluid, being ideal for the incorporation of hydrophobic entities. For prolonged blood circulation time, the biocompatible polymer PEG, covalently linked to DSPE, was included in the lipid composition. EPC:DSPE-PEG liposomes, hereafter designated as LIP HM, were homogeneous (PdI < 0.1), with a mean hydrodynamic size of around 100 nm, displaying a high HM loading (> 33 nmol/μmol of lipid) with an incorporation efficiency (I.E.) around 100%. A zeta potential close to neutrality was obtained being in accordance with the lipid composition used [34]. HM-loaded liposomes were further characterized in terms of antiproliferative activity towards the murine melanoma cell line B16-F10. An IC$_{50}$ value of 45.1 μM was obtained for Free HM after 72 h of incubation. Encapsulation of HM in liposomes decreased its cytotoxicity, with an IC$_{50}$ > 75 μM for all lipid compositions tested (Fig. 2b).

To elucidate decreased *in vitro* antiproliferative effects of LIP HM compared to its free form, a comparative assessment of possible lipid-HM interactions by nuclear magnetic resonance (NMR) analysis was performed. PC, the major component used in the lipid composition, is a fluid phospholipid, thus allowing an efficient entrapment of hydrophobic molecules in the lipid bilayer [35]. In fact, the analysis of ^{1}H NMR spectra of LIP HM (Fig. 2c and Supplementary Fig. S3) showed a higher chemical shift perturbation along the entire spectra, in comparison to HM in the free form. The signals from the linker between the two aromatic rings are completely unobserved and the signals of the aromatic rings shifted to higher field. Overall, the stable accommodation of HM within lipid bilayers may explain the differences in antiproliferative effects of free and liposomal HM. Moreover, microscopic visualization of B16-F10 cells, following incubation with rhodamine-labelled LIP HM, clearly demonstrated liposomes accumulation in cell cytoplasm, being this effect time-dependent (Supplementary Fig. S5). Similar results were obtained for non-PEGylated liposomes, suggesting that surface coating
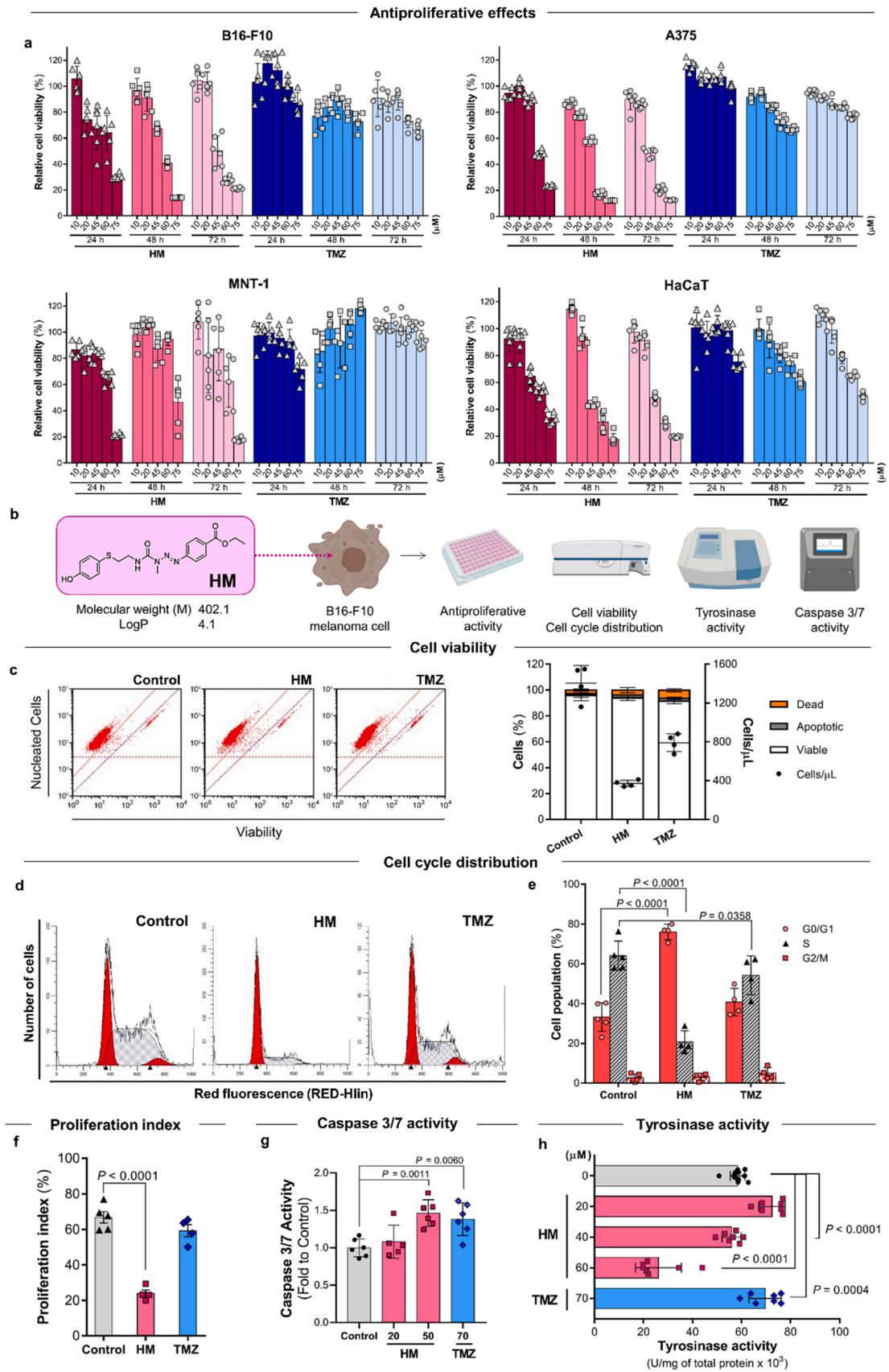
(caption on next page)

Fig. 1. Novel hybrid molecule (HM) with antitumour activity. a, Relative cell viability (%) of murine (B16-F10) and human (MNT-1 and A375) melanoma cells and normal human keratinocytes (HaCaT) 24, 48 and 72 h after incubation with HM and TMZ at concentrations ranging from 10 to 75 μM (*n* = 6). Cellular viability was determined by MTT assay. b, Schematic representation of HM biological effects studied *in vitro* on the murine melanoma cell line B16-F10. c, Representation of B16-F10 cell populations by flow cytometry 24 h after incubation with HM and TMZ at 50 and 70 μM, respectively. The column chart represents the percentage of viable, apoptotic, and dead B16-F10 cells and number of cells/μL (*n* = 4) obtained by Guava ViaCount assay. d, Representative histograms of the gated B16-F10 cells in G0/G1, S, and G2/M phases of cell cycle in the absence (Control) or presence of HM and TMZ at 50 and 70 μM, respectively. e, Quantitative analysis of B16-F10 cell proportion in each cell cycle phase obtained for 10,000 cells *per* sample. f, Proliferation indexes for HM and TMZ, determined according to cell cycle distribution of exponentially growing populations as the sum of percentage of cells in S and G2/M phases. In e and f, *n* = 5 for the Control group and *n* = 4 for treated groups. g, Caspase 3/7 activity determined from protein extracts of B16-F10 cells in the absence (Control; *n* = 6) or presence of HM at 20 (*n* = 5) and 50 μM (*n* = 6) and TMZ at 70 μM (*n* = 6), for 4 h of incubation. h, Tyrosinase activity of B16-F10 in the absence (Control; *n* = 12) or presence of HM at 20, 40 and 60 μM and TMZ at 70 μM, for 24 h (*n* = 7). Mushroom tyrosinase (1000 U/mL) was used as positive control (data not shown). Data are expressed as mean ± s.d. Statistics: two-way (e) and one-way (f, g, h) ANOVA followed by Dunnet's post-hoc test.

with the polymer does not affect liposome internalization (data not shown).

In addition, HM release kinetics in the presence of plasma were conducted. The obtained results demonstrated the high stability of loaded HM in liposomes as, 24 h after incubation in plasma, around 80% of HM was still incorporated (Supplementary Fig. S4) thus also explaining the lower cytotoxic activity *in vitro*.

The stability of LIP HM in suspension and in lyophilized form was also evaluated. When stored for 1 week at + 4 °C, LIP HM in suspension maintained the original physicochemical properties, displaying a mean size of 100 ± 1.0 nm (PdI < 0.1) and retaining 98 ± 4% of the initially incorporated HM (Fig. 2e and Supplementary Fig. S6). Furthermore, the long-term stability of liposomes may be ensured by lyophilization using appropriate cryoprotectants [29,36]. This method should guarantee that, upon rehydration, liposomes preserve their initial characteristics, such a size distribution and drug loading [29,36]. Upon 1 month of storage in the lyophilized form, in the presence of the cryoprotectant trehalose, LIP HM maintained its properties (mean size ∼ 100 nm and PdI < 0.15) and effectively retained the initially incorporated HM amount, in contrast to liposomes lyophilized without trehalose. Indeed, for HM liposomes stored in the absence of the cryoprotectant, an increase on the mean size from 103 ± 1 nm to 563 ± 47 nm, accompanied by an increase on the PdI > 0.3, was observed (Fig. 2f and Supplementary Fig. S6). Moreover, zeta potential was maintained for all formulations under storage, either in suspension or lyophilized. (Supplementary Fig. S6). The high stability of LIP HM in suspension, and in the lyophilized forms confirm the strong insertion of the molecule within the lipid bilayer of liposomes (Fig. 2d, e, f and Supplementary Fig. S4).

Taking into account that HM contains two pharmacophores, it is also important to evaluate the hydrolysis rate and formation of its sub-products. HM in the free form displayed a plasma half-life of 30 h [13], meaning that after this period of time, 50% of the hybrid compound was already decomposed in the two pharmacophoric moieties. On the other hand, after incorporation in liposomes, an increase on the plasma half-life for HM was observed (39 h), as depicted in Fig. 2d, thus demonstrating the advantages of liposomes in protecting loaded HM.

Preliminary safety assays were performed for HM formulations namely haemolytic activity after incubation with human red blood cells (hRBC). The absence of haemolysis showed the suitability of HM formulations for parenteral administration (Fig. 2d). Furthermore, this result was also confirmed *in vivo*, after i.v. administration in healthy BALB/c mice (Supplementary Fig. S7).

3.3. Therapeutic effect of HM liposomes in a subcutaneous murine melanoma model

Using an established B16-F10 syngeneic subcutaneous melanoma model [17], the antitumor effect of LIP HM was evaluated and compared with Free HM and PBS (Fig. 3a). LIP HM treatment (at 12 mg of HM/kg of body weight every other day in a total of six i.v. treatments) resulted in the strongest inhibition of melanoma tumour progression (Fig. 3b, c, d). At day 20, a 5- and 2-fold reduction in mean tumour volume were

achieved for animals treated with LIP HM (429 ± 86 mm³) and Free HM (1010 ± 310 mm³), respectively, relative to non-treated mice (2007 ± 359 mm³) (Fig. 3b). Reflecting the tumour volume evolution profiles, RTV values of 4.1 ± 0.6, 8.0 ± 2.2 and 12.4 ± 2.9 were achieved for LIP HM, Free HM and PBS groups, respectively, at day 20 after the tumour induction (Fig. 3c). At the end of the treatment protocol (day 20), mice treated with LIP HM displayed the lowest median tumour weight values (1.2 ± 0.5 g), compared to 2.0 ± 0.5 g and 3.0 ± 0.5 g for Free HM and PBS, respectively (Fig. 3d). Moreover, an increase of caspase 3/7 activity and a decrease of the tyrosinase activity were observed in protein extracts of melanoma solid tumours dissected after the last treatment with LIP HM (Fig. 3e, f), in line with the *in vitro* data described above (Fig. 1d-h).
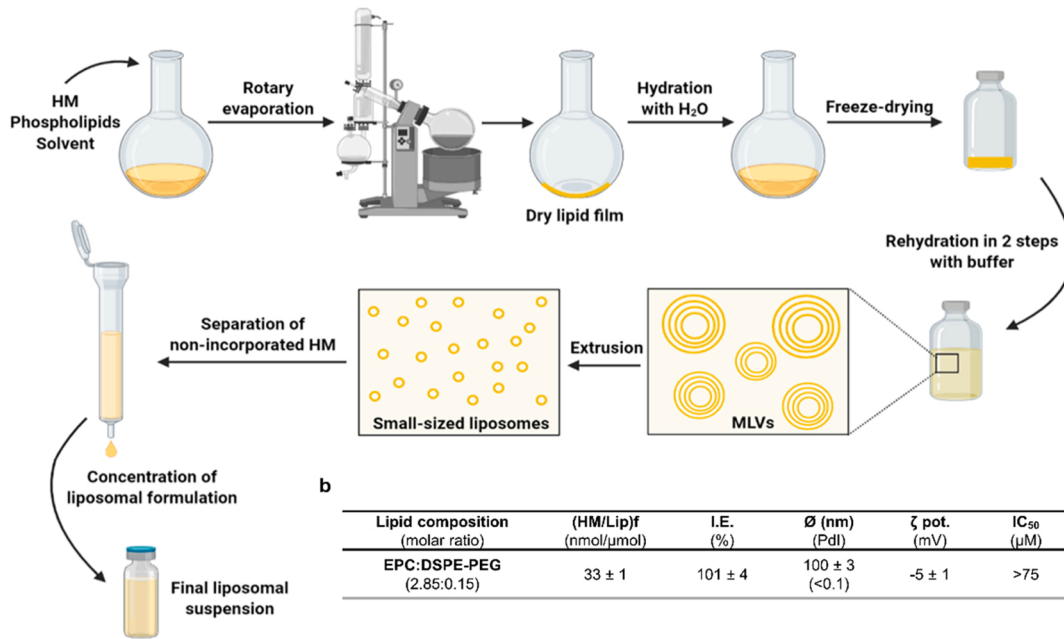
No significant changes in animal body weight (Fig. 3g) and tissue index values for liver, spleen kidney and lung were detected among all groups under study (Supplementary Fig. S8). Also, the liver enzymes alanine aminotransferase (ALT), aspartate aminotransferase (AST) and γ-glutamyl transferase (γ-GT) were within reference interval for all treatment groups [37] (Supplementary Fig. S8), thus suggesting lack of hepatic toxicity [38,39].

3.4. Therapeutic effect of HM liposomes in a metastatic murine melanoma model
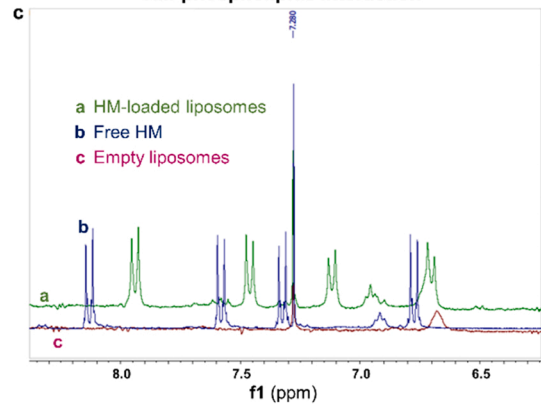
Advanced metastatic stages of melanoma are associated with high mortality and development of drug resistance [40]. Therefore, a metastatic murine melanoma model was also employed to study the antitumour activity of LIP HM. The melanoma metastases induction protocol was previously optimized by timely monitoring the development of metastases in C57BL/6 mice after i.v. injection of B16-F10 melanoma cells (Supplementary Fig. S9). B16-F10 cells have been reported to generate pulmonary and brain metastases, and is a widely used model to study new drug candidates in advanced malignancy [41]. Aiming at defining the most appropriate time for starting the treatment regimen, animal weight was monitored (Supplementary Fig. S9a) and the organs of interest, such as lungs and brains, collected for histopathological analysis (Supplementary Fig. S9b). Data confirmed the presence of lung and brain metastases 7 days after i.v. injection of B16-F10 cells, without alterations of body weight. Based on these results, the treatment schedule was initiated 1 week after tumour induction (Fig. 4a). HM was administered in free and liposomal form at a dose of 12 mg of HM/kg/treatment/day over 5 consecutive days, while TMZ, at 25 mg/kg of body weight (as reported in the literature [42,43]), was used as positive control. This drug is frequently used for patients at advanced melanoma stages with brain metastases [44].

At the end of the treatment protocol (*i.e.*, day 13 after tumour induction), macroscopic examination of the collected lungs (Fig. 4b) revealed that mice treated with LIP HM presented a score of around 1 (*i.e.*, 1–10 metastases), whereas the control PBS group displayed a score of 3 (*i.e.*, 101–200 metastases) (Fig. 4c). Also, lungs of mice receiving TMZ presented a reduction on melanoma metastasis, with a score of around 2 (*i.e.*, 11–100, metastases), although to a lesser extent than LIP HM. In the case of mice treated with Free HM, no significant reduction in lung
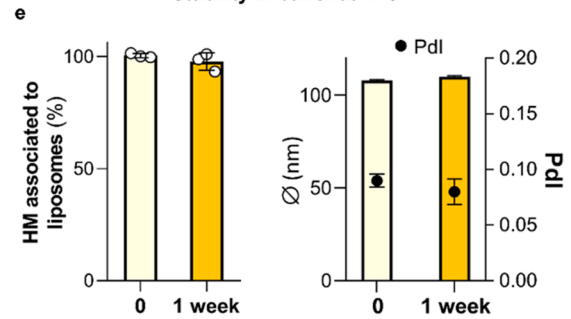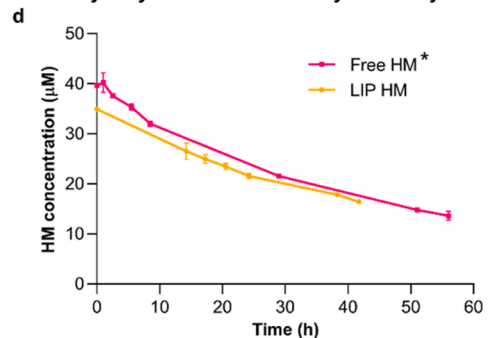
Preparation and characterization of HM liposomes

Lipid composition (molar ratio)	(HM/Lip)f (nmol/µmol)	I.E. (%)	Ø (nm) (PdI)	ζ pot. (mV)	IC50 (µM)
EPC:DSPE-PEG (2.85:0.15)	33 ± 1	101 ± 4	100 ± 3 (<0.1)	-5 ± 1	>75

HM-phospholipids interaction

c

a HM-loaded liposomes
b Free HM
c Empty liposomes

Stability in buffer at 4 °C

Hydrolysis rate and haemolytic activity

d

Formulation	$t_{1/2}$ (h)	Haemolytic activity in hRBC (%)
Free HM*	30	< 1
LIP HM	39	< 1

* Data from [13]

Stability in the lyophilized form

f

Before lyophilization
After lyophilization
○ PdI
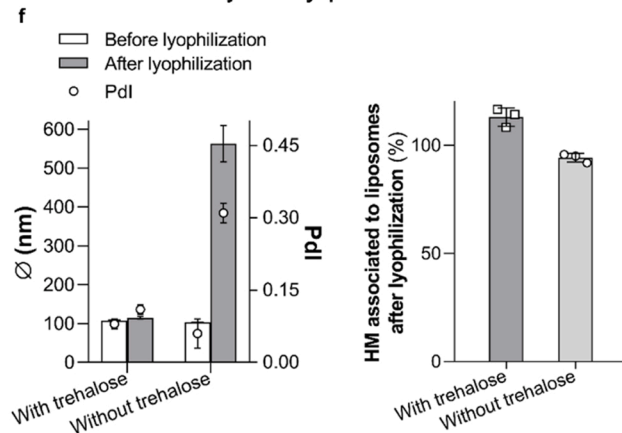
(caption on next page)

Fig. 2. Preparation, characterization, and stability of LIP HM. a, Schematic illustration of HM liposome preparation by the dehydration–rehydration method, followed by extrusion to obtain homogenous small-sized liposomes. b, Physical characterization of liposomes in terms of lipid composition, loading capacity, incorporation efficiency, mean size and zeta potential. Antiproliferative effect of HM incorporated in liposomes was evaluated towards the murine melanoma cell line B16-F10, 72 h after incubation, by MTT assay ($n = 3$). HM concentrations ranged from 10 to 75 μM. c, NMR spectra, representing LIP HM (green), Free HM (blue) and unloaded liposomes (pink) at the aromatic shift. d, Hydrolysis rate of HM in free and liposomal forms in the presence of human plasma [80% (v/v)] and haemolytic activity (%) ($n = 3$). e, f, Stability of LIP HM (EPC:DSPE-PEG) after storage at + 4 °C in suspension (e) and in the lyophilized form (f), evaluated in terms of percentage of HM associated to liposomes, mean size and PdI ($n = 3$). Results are expressed as mean ± s.d. EPC, egg phosphatidyl choline; DSPE-PEG, distearoyl phosphatidyl ethanolamine covalently linked to polyethylene glycol; I.E., incorporation efficiency; [(HM/Lip)f], loading capacity; MLVs, multilamellar vesicles; PdI, polydispersity index; $t_{1/2}$, half-life; hRBC, human red blood cells.
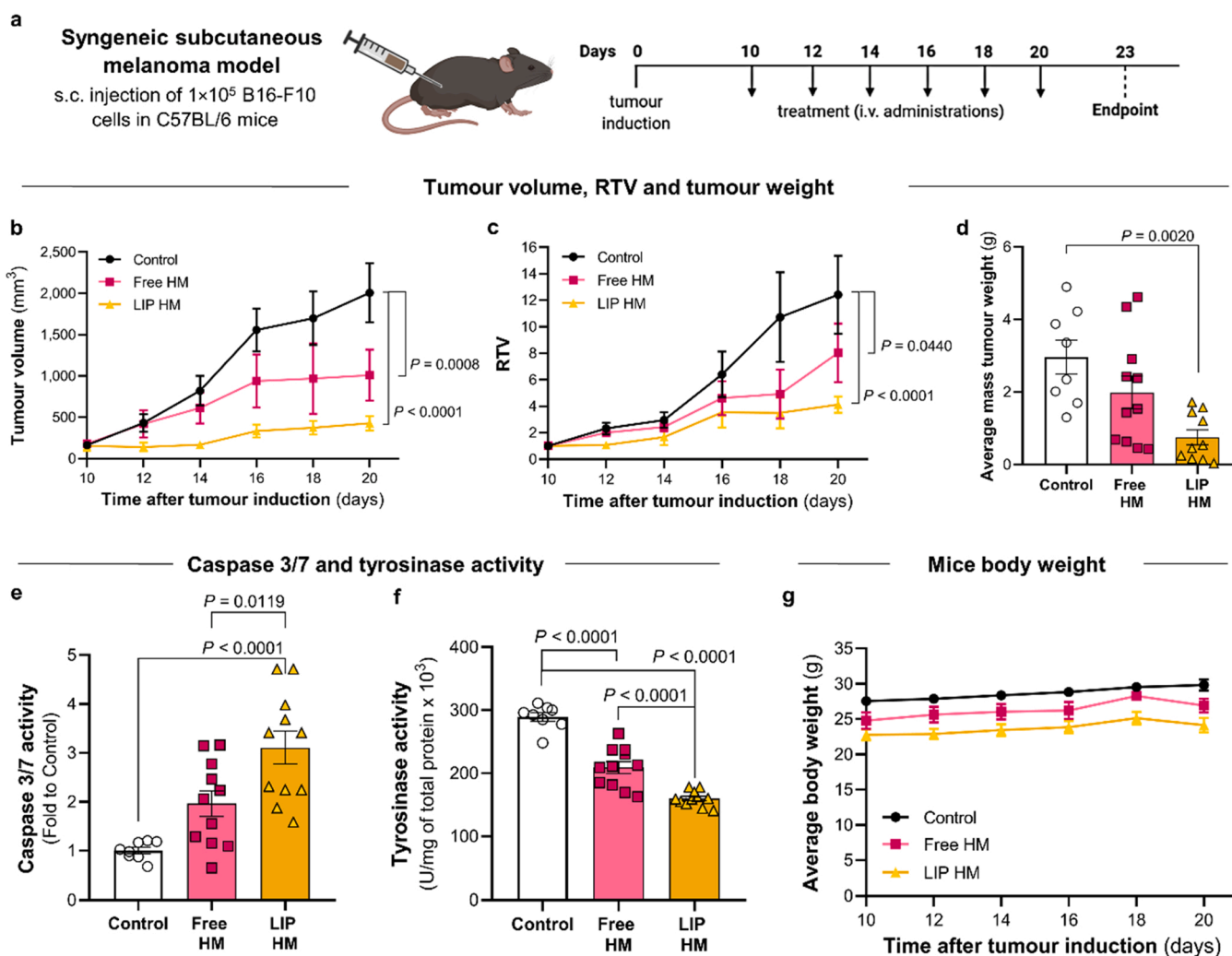

Fig. 3. Liposomal HM inhibits melanoma growth. a, Experimental protocol for the syngeneic subcutaneous melanoma murine model. 10 days after tumour induction, C57BL/6 mice were i.v. administered with PBS (non-treated control), HM in free (Free HM) or liposomal (LIP HM), at a dose of 12 mg of HM/kg of body weight every other day, in a total of six administrations. b, Tumour volume evaluation. *P* values correspond to day 20 after tumour induction. c, Relative tumour volume (RTV) for each animal, determined as the ratio between volumes at the indicated day and volumes at the beginning of the treatment. *P* values correspond to day 20 after tumour induction. d, Average mass tumours weight (g) at endpoint e, f, Caspase 3/7 activity and tyrosinase activity, respectively, determined in protein extracts from melanoma mass tumours obtained at endpoint. g, Average body weight (g) for all groups during experimental protocol. Statistics: two-way (b, c) and one-way (d, e, f) ANOVA followed by Tukey's post-hoc test.

metastases occurrence was found compared to control PBS. These results were confirmed by the histopathological analysis, as depicted in Fig. 4d. Furthermore, treatment with LIP HM led to a slight increase in caspase 3/7 activity in protein extracts from lungs when compared to the control PBS group (Fig. 4e). Such a slight increase was also identified in Free HM and TMZ treatment. However, no statistically significant differences were observed among all animal groups under study.

Regarding brain metastases, although they were not macroscopically perceptible, the histopathological analysis demonstrated that several agglomerates of cells with melanic pigment were observed in the control

PBS group *versus* small or rare clusters observed in the TMZ and Free HM treatment groups, respectively. However, after treatment with LIP HM, no microscopic lesions were noticed, suggesting that this nanoformulation exerted a stronger antitumour effect that prevented the spread of melanoma cells to the brain. During the whole experimental period, the reduction on the body weight was less than 15%, with no significant changes among groups (Fig. 4f). No alterations in brain and lung tissue index values and in hepatic parameters (AST, ALT and γ-GT) were recorded for any group under study (Supplementary Fig. S10).
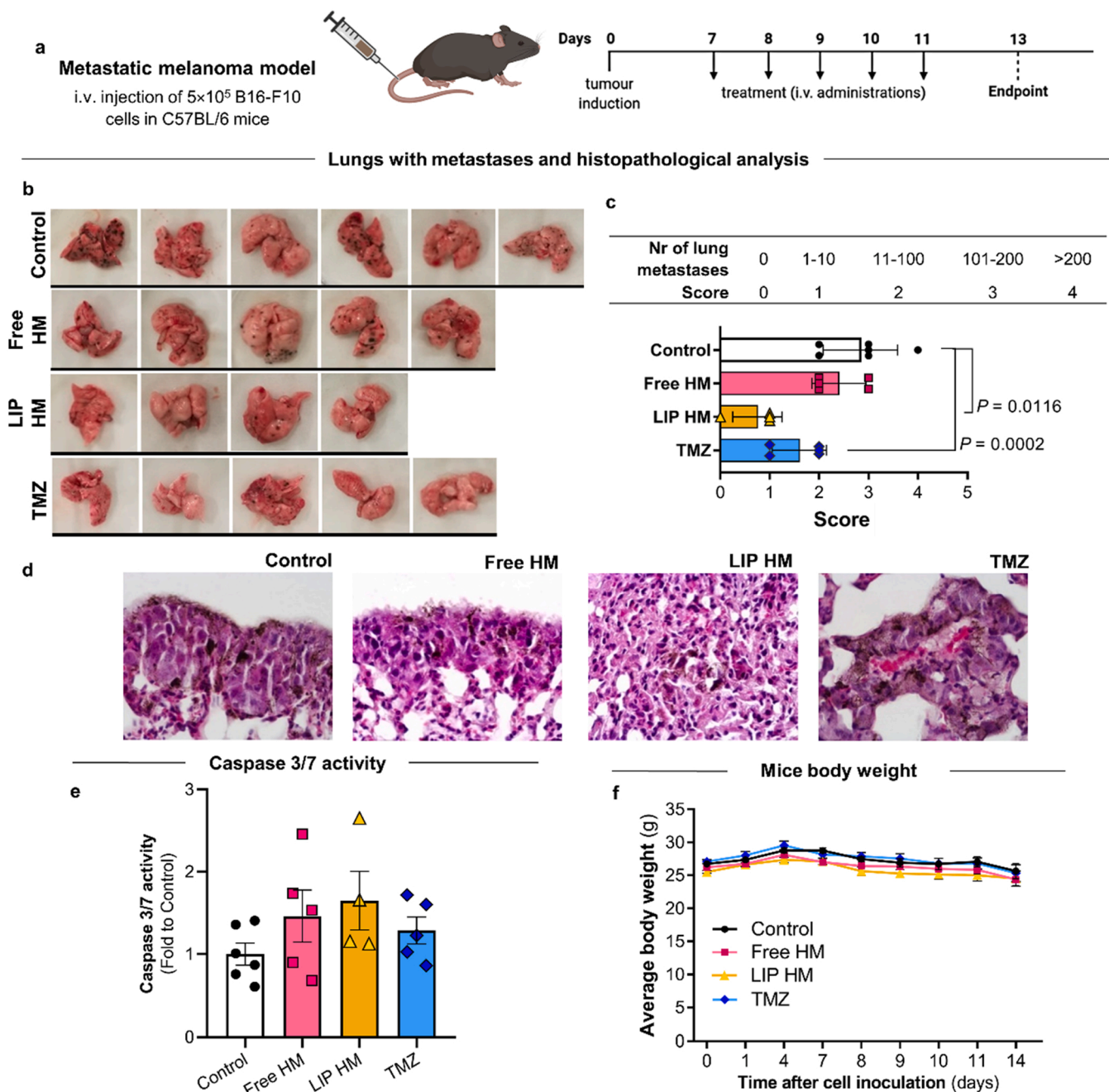
Fig. 4. Liposomal HM inhibits melanoma metastasis formation. a, Experimental set-up for the syngeneic metastatic melanoma murine model. Seven days after i.v. injection of B16-F10 melanoma cells, animals were i.v. injected with PBS (non-treated control), HM in free form (Free HM) or incorporated in liposomes (LIP HM) at a dose of 12 mg/kg of body weight, or TMZ at a dose of 25 mg/kg, for 5 consecutive days. b, Representative images of mice lungs at the experimental endpoint. The metastases are manifested as dark spots. c, Establishment of a score based on the number of lung metastases macroscopically visualized. d, Representative images from histopathological analysis of lung samples from each group; Control: multiple clusters of pleomorphic cells with melanic pigment accumulation; Free HM: multiple and dispersed clusters of pleomorphic cells with melanic pigment accumulation, in perivascular and peribronchiolar position; LIP HM: very rare and very small clusters of pleomorphic cells with melanic pigment accumulation; TMZ: small number of clusters of pleomorphic cells with melanic pigment accumulation, located in alveoli, perivascular and subpleural position. Haematoxylin and eosin and Fontana-Masson staining. Original magnification, 400x. e, Influence of HM and TMZ treatment on caspase 3/7 activity determined in protein extracts from lungs. f, Average body weight evaluation for all groups under study. Results are expressed as mean ± s.d. Statistics: one-way ANOVA (c, f) followed by Tukey's post-hoc test.

3.5. Biodistribution of ^{111}In labelled HM liposomes in murine melanoma models

To assess the biodistribution profile of LIP HM, the chelating agent DTPA was co-loaded in the liposomal aqueous interior, allowing further labelling with the radionuclide ^{111}In, as previously published [32] (Fig. 5a). ^{111}In-DTPA labelled LIP HM was administered i.v. to healthy (naive) mice (Fig. 5b) as well as to animals with metastatic (Fig. 5c) or subcutaneous (Fig. 5d, e, f) melanoma. The quantification of labelled liposomes in organs under study was performed at 1, 4, 24 and 48 h post-injection.

Liposomes, depending on the lipid composition, can extravasate through 'leaky' tumour blood vessels [45,46] and, once in tumour *interstitium*, are retained in these sites due to a deficient lymphatic
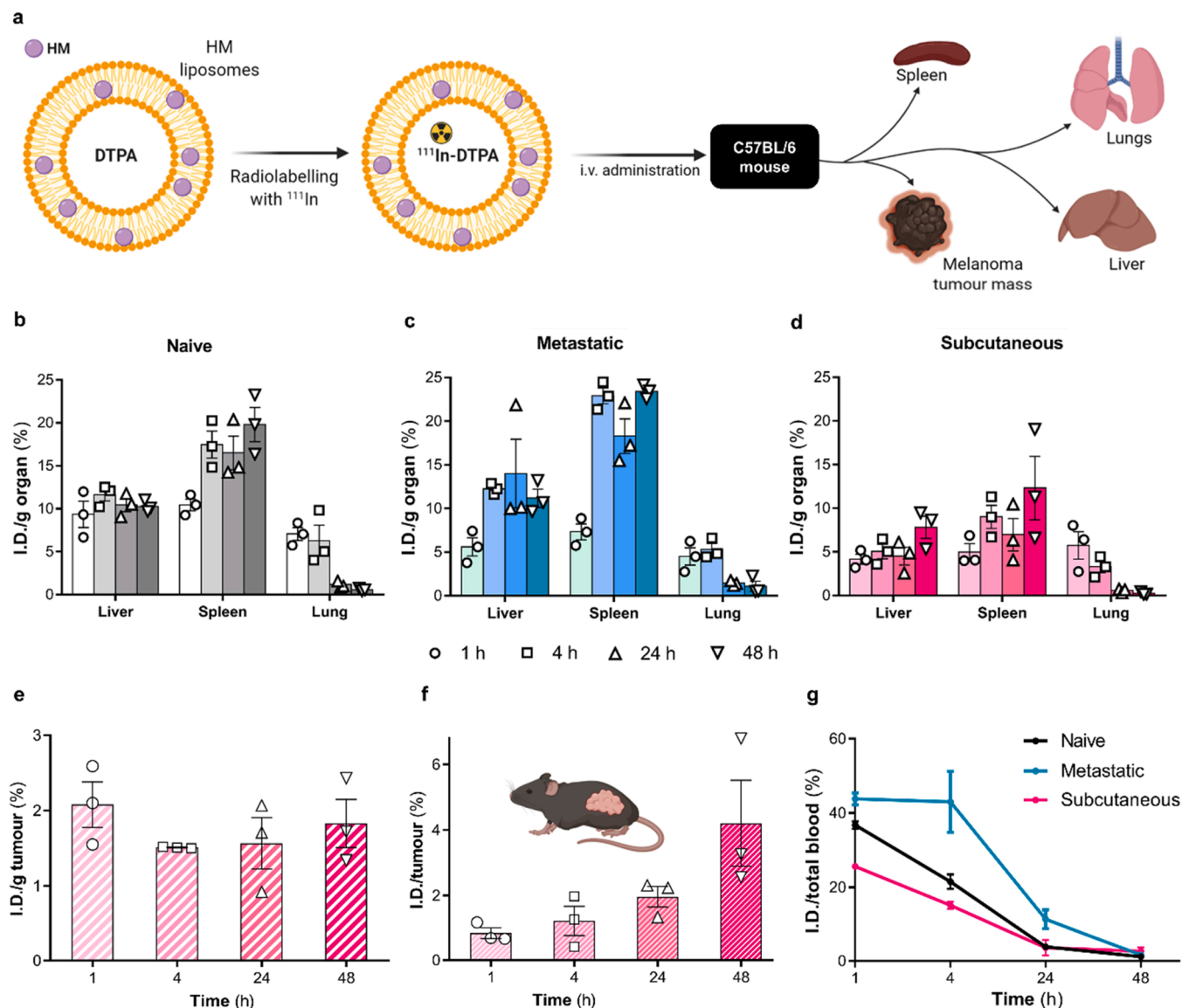
Fig. 5. Liposomal HM accumulates in melanoma tumour mass. a, Schematic representation of the biodistribution experiment. HM liposomes were co-loaded with the chelating agent DTPA and, subsequently, labelled with the radionuclide [111]In. The presence of radiolabelled HM liposomes in liver, spleen, lungs, tumour mass and blood, as a function of time, was determined after i.v. administration in C57BL/6 mice ($n = 3$). Data are expressed as percentage of I.D. *per* gram of organ in (b) healthy mice, (c) mice from syngeneic metastatic melanoma model and (d) mice from syngeneic subcutaneous melanoma model. e, f, Accumulation of the ^{111}In-DTPA labelled HM liposomes *per* gram of tumour mass (e) and total tumour mass (f) of mice from syngeneic subcutaneous melanoma model. g, Percentage of I.D. in total blood of ^{111}In-DTPA labelled HM liposomes in healthy and both melanoma mice models (subcutaneous and metastatic). DTPA: diethylenetriamine pentaacetic acid, I. D.: injected dose.

drainage system [20,45,46] *via* the widely described enhanced permeability and retention effect [46].

In the present work, DSPE-PEG was included in the lipid composition of LIP HM, to ensure a long blood circulation time, as PEG limits rapid uptake by the mononuclear phagocyte system [20,29,47]. This was confirmed by the detection of LIP HM in the bloodstream for up to 48 h post-injection (Fig. 5g). In the subcutaneous melanoma murine model, 48 h after administration of LIP HM, 4% of the injected dose was attained in the tumour (Fig. 5e, f) with a concomitant reduction in other organs (Fig. 5d and Supplementary Fig. S11 and S12), and in blood (Fig. 5g). Although some reports describe superior injected dose levels at tumour sites, (around 4%) [48,49], other pre-clinical studies exhibited less than 1% [20,50,51]. Curiously, the biodistribution profile of LIP HM in the metastatic murine melanoma model (Fig. 5c and Supplementary Fig. S11 and S12) was similar to the naive animals (Fig. 5b and Supplementary Fig. S11 and S12). The accumulation of LIP HM in major

organs may be explained by resident macrophages in liver, spleen and lungs that substantially contribute to liposomes uptake, which is in accordance with the current understanding of their biodistribution profile *in vivo* [47,52,53].

4. Discussion

Despite immeasurable progresses in medicine, malignant melanoma treatment is still a challenge due to resistance to available therapeutic options [5,54]. Current research efforts explore the use of hybrid molecules, which result from the covalent fusion of two or more distinct pharmacophores to achieve a single entity that is able to act, simultaneously, on the same or different targets [5]. Herein, we propose a strategy to improve the delivery of a potent dual acting hybrid molecule *via* passive tumour targeting based on its association to liposomes, a versatile nanotechnological tool designed and validated both *in vitro* and

in vivo.

This newly synthetized HM combines a triazene, as an alkylating moiety, and the ʟ-tyrosine analogue (4-*S*-CAP), with melanocytotoxic and immunomodulatory properties [13]. Triazenes are a class of antitumour agents that act *via* DNA alkylation, represented in the clinic by dacarbazine and TMZ, two prodrugs with different activation mechanisms [5,11,55]. While TMZ is activated by an aqueous environment at pH 7.4, dacarbazine needs cytochrome P450 isoforms (CYP1A1, CYP1A2 and CYP2E1) activation [12]. Taking into account that dacarbazine is a much better substrate to CYP in rodents than in humans, TMZ was selected in the present work as positive control, as it does not need CYP activation [12,56]. This aspect is of high importance, since CYP450 is considered the most relevant enzymatic system in the metabolism of the majority of drugs, being associated with key pharmacokinetic interactions. In addition, CYP isoenzymes may be responsible for the production of toxic metabolites [57].

On the other hand, tyrosinase is aberrantly expressed in melanoma and its increased activity is directly correlated with the degree of malignancy [12,56,58]. Considering this enzyme as a potential therapeutic target, the development of ʟ-tyrosine analogues, acting as tyrosinase substrates, has been investigated as a promising antimelanoma approach. One of the discovered classes of ʟ-tyrosine analogues are the 4-sulfur-substituted phenols, including the sulfur-amine tyrosine analogue, 4-*S*-CAP [13,59,60].

In this study, HM displayed a superior antiproliferative activity towards different tumour cell lines, particularly human and murine melanoma, compared to TMZ, a drug in clinical use for metastatic melanoma management [33]. In melanotic B16-F10 cells, the *in vitro* effect of HM was associated with cell cycle arrest in G0/G1 phase. Moreover, the increased caspase 3/7 activity (Fig. 1 g) may be related with the DNA alkylating activity of HM responsible for the cell cycle arrest at G0/G1 phase, followed by apoptosis. An increase in caspase 3/7 activity was also observed using another ʟ-tyrosine analogue, the *N*-propionyl-4-*S*-CAP in B16-F1 cells [61]. Similar cell cycle results were reported for other DNA alkylating prodrugs towards breast, prostate and lung cancer cells [62], as well as for decitabine, an approved DNA methyltransferase inhibitor, against multiple myeloma cell lines [63]. In these examples, apoptosis was also suggested to result from cell cycle arrest at the G0/G1 phase [62,63]. Also, Wichmann and co-workers have confirmed cell cycle alterations in ovarian cancer cells after incubation with a triazene-like compound [64].

A reduction on the tyrosinase activity was observed for B16-F10 cells incubated with HM, in a concentration-dependent effect. This effect may result from enzyme inhibition by metabolites, that are formed in the oxidation process [13], or by a decrease in gene expression of the enzyme due to inhibition of DNA synthesis promoted by 4-*S*-CAP [65]. Further studies are required to determine which one of these mechanisms is implicated in the reduced tyrosinase activity observed.

Despite the obvious advantages and success of hybrid molecules, the *in vivo* therapeutic performance of these agents will depend on many factors, such as biodistribution profile, drug solubility, premature degradation, and associated toxic side effects. Owing to continuous progress in chemistry, pharmacology, and nanotechnology, some of the current obstacles may be overcome by using appropriate delivery systems. In previous research work, liposomal formulations of a triazene analogue exhibited higher cytotoxicity towards the human melanoma cell line, MNT-1, compared to the free compound [9]. Regarding 4-*S*-CAP moiety, it has been reported that cationic liposomes loading this ʟ-tyrosine analogue, combined with hyperthermia, suppressed B16 tumour growth [15,66].

Herein, to maximize the antimelanoma effects of HM, this dual acting molecule was successfully loaded in nanosized long blood circulating liposomes (~100 nm), with suitable incorporation parameters. When designing liposomes as drug carriers, it is vital to ensure that the associated molecule retains its structure and pharmacological activity and that the nanosystem is able to circulate in the bloodstream long

enough to reach target sites and, subsequently, release the incorporated drug. Here, liposomes surface was coated with DSPE-PEG, forming a protective shell that minimizes the binding of plasma proteins, such as opsonins, thus preventing premature blood clearance by the mononuclear phagocyte system [20,29,47]. The main phospholipid for the preparation of LIP HM was PC that was able to stably accommodate the hybrid compound within lipid bilayers, protecting it from premature degradation, and solving solubility problems. Also, it is noteworthy that a long-term stability of LIP HM was achieved in the lyophilized form, an important factor to consider when developing a product for potential clinical application.

Of note, *in vitro* results showed a lower antiproliferative activity of liposomal HM, compared to free compound. This effect might be due to the strong interaction between HM and lipid bilayers as suggested by NMR studies. However, despite the valuable information provided by *in vitro* studies regarding HM biological activity and mechanistic action, these assays do not accurately simulate the melanoma complexity, organization, and microenvironment. Therefore, biodistribution studies and therapeutic effect of LIP HM are crucial preclinical assays.

The therapeutic effect of this highly stable HM liposomal formulation was evaluated in murine models of primary and metastatic melanoma. In the subcutaneous model, LIP HM remarkably impaired tumour progression, compared to other treated groups, devoid of toxic side effects. Importantly, biodistribution studies clearly demonstrated a preferential accumulation of a considerable percentage of liposomes at tumour sites, thus explaining the observed therapeutic activity. A remarkable antitumour effect was also accomplished by LIP HM in a metastatic melanoma model, by significantly decreasing lung metastases when compared to TMZ, the positive control. These data are particularly important since this model most closely mimics the human pathology at advanced stages of the disease characterized by increased aggressiveness, resistance to treatment, and high mortality rates.

Our proposed nanotechnological approach offers an inexpensive, safe, and effective clinical alternative to existing antimelanoma chemotherapies characterized by low efficacy, reduced specificity and undesirable severe side effects. Still, the complexity of nanotechnology demands specific regulatory guidelines that must be carefully revised and updated case-by-case.

5. Conclusions

In the present work a novel hybrid molecule, HM, was validated as a potent antimelanoma agent, benefiting from the combination of DNA alkylating properties of triazenes, already present in the clinical setting, and the specificity towards tyrosinase, that is overexpressed at melanoma cells. We further harnessed HM antimelanoma potential by designing long blood circulating liposomes for *in vivo* applications. Data from subcutaneous and metastatic murine melanoma models revealed a huge and significant therapeutic effect of LIP HM, compared to control group or animals receiving HM in the free form, thus confirming the advantages of using liposomes as a nanoplatform for enhancing the accumulation of HM towards tumour sites. This was validated by biodistribution studies that clearly exhibited high levels of LIP HM at tumour sites (up to 4% of I.D./tumour). Altogether, this research work constitutes a strong basis for the successful progression of HM liposomes from the preclinical stage to clinical trials, aiming to reach the approval of a novel, safe, site-specific and effective treatment for melanoma.

CRediT authorship contribution statement

Jacinta O. Pinho: Formal analysis, Investigation, Writing – original draft. **Mariana Matias:** Formal analysis, Investigation, Writing – original draft. **Vanda Marques:** Methodology. **Carla Eleutério:** Methodology. **Célia Fernandes:** Methodology. **Lurdes Gano:** Methodology. **Joana D. Amaral:** Investigation, Writing – original draft. **Eduarda Mendes:** Methodology. **Maria Jesus Perry:** Methodology. **João Nuno**

Conflict of interest statement

The authors report there are no competing interests to declare.

Data Availability

Data will be made available on request.

Acknowledgements

Appendix A. Supporting information

Supplementary data associated with this article can be found in the online version at doi:10.1016/j.biopha.2022.114021.

References

[1] F. Dimitriou, R. Krattinger, E. Ramelyte, M.J. Barysch, S. Micaletto, R. Dummer, S. M. Goldinger, The world of melanoma: epidemiologic, genetic, and anatomic differences of melanoma across the globe, Curr. Oncol. Rep. 20 (2018) 87, https://doi.org/10.1007/s11912-018-0732-8.

[2] J.O. Pinho, M. Matias, M.M. Gaspar, Emergent nanotechnological strategies for systemic chemotherapy against melanoma, Nanomaterials 9 (2019) 1455, https://doi.org/10.3390/nano9101455.

[3] A.K.A. Bass, M.S. El-Zoghbi, E.-S.M. Nageeb, M.F.A. Mohamed, M. Badr, G.E.-D. A. Abuo-Rahma, Comprehensive review for anticancer hybridized multitargeting HDAC inhibitors, Eur. J. Med. Chem. 209 (2021), 112904, https://doi.org/10.1016/j.ejmech.2020.112904.

[4] M. Matias, S. Silvestre, A. Falcao, G. Alves, Recent highlights on molecular hybrids potentially useful in central nervous system disorders, Mini-Rev. Med. Chem. 17 (2017) 486–517, https://doi.org/10.2174/1389557517666161111110121.

[5] A.P. Francisco, E. Mendes, A.R. Santos, M.J. Perry, Anticancer triazenes: from bioprecursors to hybrid molecules, Curr. Pharm. Des. 25 (2019) 1623–1642, https://doi.org/10.2174/1381612825666190617155749.

[6] V.Kumar Shalini, Have molecular hybrids delivered effective anti-cancer treatments and what should future drug discovery focus on? Expert Opin. Drug Discov. (2020) 1–29, https://doi.org/10.1080/17460441.2021.1850686.

[7] R.M. Stone, P.W. Manley, R.A. Larson, R. Capdeville, Midostaurin: its odyssey from discovery to approval for treating acute myeloid leukemia and advanced systemic mastocytosis, Blood Adv. 2 (2018) 444–453, https://doi.org/10.1182/bloodadvances.2017011080.

[8] S. Karmakar, H. Kostrhunova, T. Ctvrtlikova, V. Novohradsky, D. Gibson, V. Brabec, Platinum(IV)-estramustine multiaction prodrugs are effective antiproliferative agents against prostate cancer cells, J. Med. Chem. 63 (2020) 13861–13877, https://doi.org/10.1021/acs.jmedchem.0c01400.

[9] S. Calado, C. Eleutério, E. Mendes, M. de, J. Rocha, A.P. Francisco, M.M. Gaspar, Nanoformulations of a Triazene analogue with specific affinity to human melanoma, J. Nanosci. Adv. Technol. 1 (2016) 1–9, https://doi.org/10.24218/jnat.2016.16.

[10] A. Sousa, F. Santos, M.M. Gaspar, S. Calado, J.D. Pereira, E. Mendes, A. P. Francisco, M.J. Perry, The selective cytotoxicity of new triazene compounds to human melanoma cells, Bioorg. Med. Chem. 25 (2017) 3900–3910, https://doi.org/10.1016/j.bmc.2017.04.049.

[11] F. Marchesi, M. Turriziani, G. Tortorelli, G. Avvisati, F. Torino, L. Devecchis, Triazene compounds: mechanism of action and related DNA repair systems, Pharmacol. Res. 56 (2007) 275–287, https://doi.org/10.1016/j.phrs.2007.08.003.

[12] M.F.G. Stevens, Temozolomide: from cytotoxic to molecularly-targeted agent, in: S. B.T.-C.D.D. and D. Neidle (Ed.), Cancer Drug Des. Discov, Elsevier, New York, 2008, pp. 157–172, https://doi.org/10.1016/B978-012369448-5.50010-0.

[13] M. Granada, E. Mendes, M.J. Perry, M.J. Penetra, M.M. Gaspar, J.O. Pinho, S. Serra, C.T. António, A.P. Francisco, Sulfur analogues of tyrosine in the development of triazene hybrid compounds: a new strategy against melanoma, ACS Med. Chem. Lett. 12 (2021) 1669–1677, https://doi.org/10.1021/acsmedchemlett.1c00252.

[14] X. Lai, H.J. Wichers, M. Soler-Lopez, B.W. Dijkstra, Structure and function of human tyrosinase and tyrosinase-related proteins, Chemistry 24 (2018) 47–55, https://doi.org/10.1002/chem.201704410.

[15] A. Ito, M. Fujioka, T. Yoshida, K. Wakamatsu, S. Ito, T. Yamashita, K. Jimbow, H. Honda, 4-S-Cysteaminylphenol-loaded magnetite cationic liposomes for combination therapy of hyperthermia with chemotherapy against malignant melanoma, Cancer Sci. 98 (2007) 424–430, https://doi.org/10.1111/j.1349-7006.2006.00382.x.

[16] C. Beiu, C. Giurcaneanu, A.M. Grumezescu, A.M. Holban, L.G. Popa, M.M. Mihai, Nanosystems for improved targeted therapies in melanoma, J. Clin. Med. 9 (2020) 318, https://doi.org/10.3390/jcm9020318.

[17] J.O. Pinho, J.D. Amaral, R.E. Castro, C.M.P. Rodrigues, A. Casini, G. Soveral, M. M. Gaspar, Copper complex nanoformulations featuring highly promising therapeutic potential in murine melanoma models, Nanomedicine 14 (2019) 835–850, https://doi.org/10.2217/nnm-2018-0388.

[18] M.M. Gaspar, A. Radomska, O.L. Gobbo, U. Bakowsky, M.W. Radomski, C. Ehrhardt, Targeted delivery of transferrin-conjugated liposomes to an orthotopic model of lung cancer in nude rats, J. Aerosol Med. Pulm. Drug Deliv. 25 (2012) 310–318, https://doi.org/10.1089/jamp.2011.0928.

[19] L.N. Borgheti-Cardoso, J.S.R. Viegas, A.V.P. Silvestrini, A.L. Caron, F.G. Praça, M. Kravicz, M.V.L.B. Bentley, Nanotechnology approaches in the current therapy of skin cancer, Adv. Drug Deliv. Rev. 153 (2020) 109–136, https://doi.org/10.1016/j.addr.2020.02.005.

[20] L. Belfiore, D.N. Saunders, M. Ranson, K.J. Thurecht, G. Storm, K.L. Vine, Towards clinical translation of ligand-functionalized liposomes in targeted cancer therapy: Challenges and opportunities, J. Control. Release 277 (2018) 1–13, https://doi.org/10.1016/j.jconrel.2018.02.040.

[21] D. Papahadjopoulos, T.M. Allen, A. Gabizon, E. Mayhew, K. Matthay, S.K. Huang, K.D. Lee, M.C. Woodle, D.D. Lasic, C. Redemann, Sterically stabilized liposomes: improvements in pharmacokinetics and antitumor therapeutic efficacy, Proc. Natl. Acad. Sci. USA 88 (1991) 11460–11464, https://doi.org/10.1073/pnas.88.24.11460.

[22] J.M. Harris, R.B. Chess, Effect of pegylation on pharmaceuticals, Nat. Rev. Drug Discov. 2 (2003) 214–221, https://doi.org/10.1038/nrd1033.

[23] T.M. Allen, P.R. Cullis, Drug delivery systems: entering the mainstream, Science 303 (80-.) (2004) 1818–1822.

[24] N.A. Fonseca, A.C. Gregório, V.M. Mendes, R. Lopes, T. Abreu, N. Gonçalves, B. Manadas, M. Lacerda, P. Figueiredo, M. Pereira, M. Gaspar, F. Colelli, D. Pesce, G. Signorino, L. Focareta, A. Fucci, F. Cardile, C. Pisano, T. Cruz, L. Almeida, V. Moura, S. Simões, J.N. Moreira, GMP-grade nanoparticle targeted to nucleolin downregulates tumor molecular signature, blocking growth and invasion, at low systemic exposure, Nano Today 37 (2021), 101095, https://doi.org/10.1016/j.nantod.2021.101095.

[25] D.J.A. Crommelin, P. van Hoogevest, G. Storm, The role of liposomes in clinical nanomedicine development. What now? Now what? J. Control. Release 318 (2020) 256–263, https://doi.org/10.1016/j.jconrel.2019.12.023.

[26] J.I. Hare, T. Lammers, M.B. Ashford, S. Puri, G. Storm, S.T. Barry, Challenges and strategies in anti-cancer nanomedicine development: an industry perspective, Adv. Drug Deliv. Rev. 108 (2017) 25–38, https://doi.org/10.1016/j.addr.2016.04.025.

[27] S. Shah, V. Dhawan, R. Holm, M.S. Nagarsenker, Y. Perrie, Liposomes: advancements and innovation in the manufacturing process, Adv. Drug Deliv. Rev. 154–155 (2020) 102–122, https://doi.org/10.1016/j.addr.2020.07.002.

[28] M. Houshmand, F. Garello, P. Circosta, R. Stefania, S. Aime, G. Saglio, C. Giachino, Nanocarriers as magic bullets in the treatment of leukemia, Nanomaterials 10 (2020) 276, https://doi.org/10.3390/nano10020276.

[29] M.M. Gaspar, S. Calado, J. Pereira, H. Ferronha, I. Correia, H. Castro, A.M. Tomás, M.E.M. Cruz, Targeted delivery of paromomycin in murine infectious diseases through association to nano lipid systems, Nanomed. Nanotechnol. Biol. Med. 11 (2015) 1851–1860, https://doi.org/10.1016/j.nano.2015.06.008.

[30] G. Rouser, S. Fleischer, A. Yamamoto, Two dimensional thin layer chromatographic separation of polar lipids and determination of phospholipids by phosphorus analysis of spots, Lipids 5 (1970) 494–496, https://doi.org/10.1007/BF02531316.

[31] M. Nave, R.E. Castro, C.M.P. Rodrigues, A. Casini, G. Soveral, M.M. Gaspar, Nanoformulations of a potent copper-based aquaporin inhibitor with cytotoxic effect against cancer cells, Nanomedicine 11 (2016) 1817–1830, https://doi.org/10.2217/nnm-2016-0086.

[32] M.M. Gaspar, O.C. Boerman, P. Laverman, M.L. Corvo, G. Storm, M.E.M. Cruz, Enzymosomes with surface-exposed superoxide dismutase: in vivo behaviour and therapeutic activity in a model of adjuvant arthritis, J. Control. Release 117 (2007) 186–195, https://doi.org/10.1016/j.jconrel.2006.10.018.

[33] Z. Tatar, E. Thivat, E. Planchat, P. Gimbergues, E. Gadea, C. Abrial, X. Durando, Temozolomide and unusual indications: review of literature, Cancer Treat. Rev. 39 (2013) 125–135, https://doi.org/10.1016/j.ctrv.2012.06.002.

[34] M.A. Phillips, M.L. Gran, N.A. Peppas, Targeted nanodelivery of drugs and diagnostics, Nano Today 5 (2010) 143–159, https://doi.org/10.1016/j.nantod.2010.03.003.

[35] M.M. Gaspar, S. Neves, F. Portaels, J. Pedrosa, M.T. Silva, M.E.M. Cruz, Therapeutic efficacy of liposomal rifabutin in a Mycobacterium avium model of infection, Antimicrob. Agents Chemother. 44 (2000) 2424–2430, https://doi.org/10.1128/AAC.44.9.2424-2430.2000.

[36] E.C. van Winden, W. Zhang, D.J. Crommelin, Effect of freezing rate on the stability of liposomes during freeze-drying and rehydration, Pharm. Res 14 (1997) 1151–11560, https://doi.org/10.1023/a:1012142520912.

[37] Charles River Laboratories, C57BL/6 Mice, (2012). ⟨https://www.criver.com/sites/default/files/resources/C57BL6MouseClinicalPathologyData.pdf⟩ (Accessed November 25, 2020).

[38] M.C. Kew, Serum aminotransferase concentration as evidence of hepatocellular damage, Lancet 355 (2000) 591–592, https://doi.org/10.1016/S0140-6736(99)00219-6.

[39] J.R. Senior, Evolution of the food and drug administration approach to liver safety assessment for new drugs: current status and challenges, Drug Saf. 37 (2014) 9–17, https://doi.org/10.1007/s40264-014-0182-7.

[40] M.B. Arasi, F. Pedini, S. Valentini, N. Felli, F. Felicetti, Advances in natural or synthetic nanoparticles for metastatic melanoma therapy and diagnosis, Cancers 12 (2020) 2893, https://doi.org/10.3390/cancers12102893.

[41] G.K. Couto, N.V. Segatto, T.L. Oliveira, F.K. Seixas, K.M. Schachtschneider, T. Collares, The melding of drug screening platforms for melanoma, Front. Oncol. 9 (2019) 512, https://doi.org/10.3389/fonc.2019.00512.

[42] T. Viel, S. Schelhaas, S. Wagner, L. Wachsmuth, K. Schwegmann, M. Kuhlmann, C. Faber, K. Kopka, M. Schäfers, A.H. Jacobs, Early assessment of the efficacy of temozolomide chemotherapy in experimental glioblastoma using [18F]FLT-PET imaging, PLoS One 8 (2013), e67911, https://doi.org/10.1371/journal.pone.0067911.

[43] D. Saha, S.D. Rabkin, R.L. Martuza, Temozolomide antagonizes oncolytic immunovirotherapy in glioblastoma, J. Immunother. Cancer 8 (2020), e000345, https://doi.org/10.1136/jitc-2019-000345.

[44] L. Kuryk, L. Bertinato, M. Staniszewska, K. Pancer, M. Wieczorek, S. Salmaso, P. Caliceti, M. Garofalo, From conventional therapies to immunotherapy: Melanoma treatment in review, Cancers 12 (2020) 3057, https://doi.org/10.3390/cancers12103057.

[45] M.E.M. Cruz, S.I. Simões, M.L. Corvo, M.B.F. Martins, M.M. Gaspar, Formulation of NPDDS for macromolecules, in: Y. Pathak, D. Thassu (Eds.), Drug Deliv. Nanoparticles Formul. Charact., Informa Healthcare, New York, USA, 2009, pp. 35–49.

[46] H. Maeda, J. Wu, T. Sawa, Y. Matsumura, K. Hori, Tumor vascular permeability and the EPR effect in macromolecular therapeutics: a review, in: J. Control. Release, 65, 2000, pp. 271–284.

[47] F. Perche, V.P. Torchilin, Recent trends in multifunctional liposomal nanocarriers for enhanced tumor targeting, J. Drug Deliv. 2013 (2013) 1–32, https://doi.org/10.1155/2013/705265.

[48] C.M. Dawidczyk, L.M. Russell, M. Hultz, P.C. Searson, Tumor accumulation of liposomal doxorubicin in three murine models: optimizing delivery efficiency, Nanomed., Biol. Med 13 (2017) 1637–1644, https://doi.org/10.1016/j.nano.2017.02.008.

[49] J.N. Moreira, R. Gaspar, T.M. Allen, Targeting stealth liposomes in a murine model of human small cell lung cancer, Biochim. Biophys. Acta - Biomembr. 1515 (2001) 167–176, https://doi.org/10.1016/S0005-2736(01)00411-4.

[50] S. Wilhelm, A.J. Tavares, Q. Dai, S. Ohta, J. Audet, H.F. Dvorak, W.C.W. Chan, Analysis of nanoparticle delivery to tumours, Nat. Rev. Mater. 1 (2016) 16014, https://doi.org/10.1038/natrevmats.2016.14.

[51] S. Sindhwani, A.M. Syed, J. Ngai, B.R. Kingston, L. Maiorino, J. Rothschild, P. MacMillan, Y. Zhang, N.U. Rajesh, T. Hoang, J.L.Y. Wu, S. Wilhelm, A. Zilman, S. Gadde, A. Sulaiman, B. Ouyang, Z. Lin, L. Wang, M. Egeblad, W.C.W. Chan, The entry of nanoparticles into solid tumours, Nat. Mater. 19 (2020) 566–575, https://doi.org/10.1038/s41563-019-0566-2.

[52] E. Blanco, H. Shen, M. Ferrari, Principles of nanoparticle design for overcoming biological barriers to drug delivery, Nat. Biotechnol. 33 (2015) 941–951, https://doi.org/10.1038/nbt.3330.

[53] T.M. Allen, P.R. Cullis, Liposomal drug delivery systems: from concept to clinical applications, Adv. Drug Deliv. Rev. 65 (2013) 36–48, https://doi.org/10.1016/j.addr.2012.09.037.

[54] A.M. Matos, A.P. Francisco, Targets, structures, and recent approaches in malignant melanoma chemotherapy, ChemMedChem 8 (2013) 1751–1765, https://doi.org/10.1002/cmdc.201300248.

[55] M.F.G. Stevens, Temozolomide: from cytotoxic to molecularly-targeted agent, in: Cancer Drug Des. Discov, Elsevier, 2008, pp. 157–172, https://doi.org/10.1016/B978-012369448-5.50010-0.

[56] L.L.H. Tsang, C.P. Quarterman, A. Gescher, J.A. Slack, Comparison of the cytotoxicity in vitro of temozolomide and dacarbazine, prodrugs of 3-methyl-(triazen-1-yl)imidazole-4-carboxamide, Cancer Chemother. Pharmacol. 27 (1991) 342–346, https://doi.org/10.1007/BF00688855.

[57] M. Matias, C. Canário, S. Silvestre, A. Falcão, G. Alves, Cytochrome P450-mediated toxicity of therapeutic drugs, in: J. Wu (Ed.), Cytochrome P450 Enzym. Biochem. Pharmacol. Heal. Implic., Nova Science Publishers, 2014, pp. 13–50.

[58] A.J. Vargas, S. Sittadjody, T. Thangasamy, E.E. Mendoza, K.H. Limesand, R. Burd, Exploiting tyrosinase expression and activity in melanocytic tumors, Integr. Cancer Ther. 10 (2011) 328–340, https://doi.org/10.1177/1534735410391661.

[59] I. Shosuke, K. Toshiaki, I. Kiichi, K. Tsutomu, J. Kowichi, Mechanism of selective toxicity of 4-S-cysteinylphenol and 4-S-cysteaminylphenol to melanocytes, Biochem. Pharmacol. 36 (1987) 2007–2011, https://doi.org/10.1016/0006-2952(87)90501-6.

[60] T. Miura, K. Jimbow, S. Ito, The in vivo antimelanoma effect of 4-S-cysteaminyl-phenol and its N-acetyl derivative, Int. J. Cancer 46 (1990) 931–934, https://doi.org/10.1002/ijc.2910460530.

[61] Y. Ishii-Osai, T. Yamashita, Y. Tamura, N. Sato, A. Ito, H. Honda, K. Wakamatsu, S. Ito, E. Nakayama, M. Okura, K. Jimbow, N-propionyl-4-S-cysteaminylphenol induces apoptosis in B16F1 cells and mediates tumor-specific T-cell immune responses in a mouse melanoma model, J. Dermatol. Sci. 67 (2012) 51–60, https://doi.org/10.1016/j.jdermsci.2012.04.009.

[62] G.A. Vielhauer, M. Swink, N.K. Parelkar, J.P. Lajiness, A.L. Wolfe, D. Boger, Evaluation of a reductively activated duocarmycin prodrug against murine and human solid cancers, Cancer Biol. Ther. 14 (2013) 527–536, https://doi.org/10.4161/cbt.24348.

[63] K. Maes, M. Lemaire, J. Gauthier, H. De Raeve, E. Menu, E. Van Valckenborgh, H. J. Wiklund, K. Vanderkerken, E. De Bruyne, The DNA methyltransferase inhibitor decitabine induces DNA damage, cell cycle arrest and apoptosis in multiple myeloma, Blood 120 (2012) 1833, https://doi.org/10.1182/blood.V120.21.1833.1833.

[64] C. Wichmann, D.M. Klotz, H.-J. Zeiler, R.A. Hilger, K. Grützmann, A. Krüger, D. Aust, P. Wimberger, J.D. Kuhlmann, The effect of the triazene compound CT913 on ovarian cancer cells in vitro and its synergistic interaction with the PARP-inhibitor olaparib, Gynecol. Oncol. (2020), https://doi.org/10.1016/j.ygyno.2020.09.018.

[65] P.D. Thomas, H. Kishi, H. Cao, M. Ota, T. Yamashita, S. Singh, K. Jimbow, Selective incorporation and specific cytocidal effect as the cellular basis for the antimelanoma action of sulphur containing tyrosine analogs, J. Invest. Dermatol. 113 (1999) 928–934, https://doi.org/10.1046/j.1523-1747.1999.00781.x.

[66] T. Takada, T. Yamashita, M. Sato, A. Sato, I. Ono, Y. Tamura, N. Sato, A. Miyamoto, A. Ito, H. Honda, K. Wakamatsu, S. Ito, K. Jimbow, Growth inhibition of re-challenge B16 melanoma transplant by conjugates of melanogenesis substrate and magnetite nanoparticles as the basis for developing melanoma-targeted chemo-thermo-immunotherapy, J. Biomed. Biotechnol. 2009 (2009) 1–13, https://doi.org/10.1155/2009/457936.